ISSN 2070-2051, Protection of Metals and Physical Chemistry of Surfaces, 2024, Vol. 60, No. 4, pp. 723–733. © Pleiades Publishing, Ltd., 2024.

NEW SUBSTANCES, MATERIALS AND COATINGS

Effects of Minor Al, Ag, and Sb Additions on the Thermal, Microstructure and Microhardness of Zn–Sn–Cu–Bi High-Temperature Solder Alloys

Sezen Aksöz[a], *, Pınar Ata Esener[b], Esra Öztürk[c], and Necmettin Maraşlı[d]

[a] *Department of Physics, Nevşehir Hacı Bektaş Veli University, Nevşehir, 50300 Turkey*

[b] *Graduate School of Natural and Applied Sciences, Erciyes University, Kayseri, 38039 Turkey*

[c] *Department of Physics, Kocaeli University, Kocaeli, 41380 Turkey*

[d] *Department of Aeronautical Engineering, Faculty of Engineering and Architecture, İstanbul Gelişim University, Avcılar, İstanbul, 34310 Turkey*

**e-mail: sezenaksoz@nevsehir.edu.tr*

Received February 23, 2023; revised January 11, 2024; accepted February 12, 2024

Abstract—In the present study, the changes in microstructure, thermal conductivity (*K*), melting properties and microhardness (*HV*) adding of 0.05 wt % Al, Ag and Sb into Zn–5Sn–2Cu–1.5Bi (ZSCB) high temperature solder alloy were investigated. The addition of trace amounts of Al, Ag and Sb caused a significant improvement in *K* and *HV* values. Addition of 0.05 wt % of Al and Ag into the ZSCB alloy increased the *K* and *HV* values by 62% and in the range of 19–21%, respectively. The addition of 0.05 wt % of Sb increased the *K* and *HV* values by 32 and 36%, respectively.

Keywords: microhardness, microstructure, high-temperature solder alloys, thermal conductivity

DOI: 10.1134/S2070205124701934

INTRODUCTION

After understanding the irreversible damage of lead to human health and the environment, the use and development of lead-free solder alloys has gained importance over time. New lead-free solder alloys have begun to be used as an alternative to traditional high-temperature lead-containing solder alloys. However, these alloys do not fully meet all the requirements. The understanding and development of the properties of these alternative alloys in high temperature applications has been the motivation point for this field. For these soldering alloys, Zn–Sn, Au–Sn and bismuth-based alloys can be considered as the three main candidate alloys. Each alloy has its own characteristics, advantages, and disadvantages. but they are considered usable for high temperature applications [1].

The development of these innovative materials sensitive to joining temperatures [2–5] for shape memory alloys and piezoelectric ceramic materials is of great importance. When soldering these materials, the joining temperature (500°C) is always above the transition temperature range, which will lead to magnetic conversion of the ceramic and deterioration of the shape memory properties of these materials [6–8]. Due to the necessity of soldering these materials, studies have been carried out to develop low-cost solders with the most suitable melting temperature. Among the potential candidates [1, 9, 10] in studies on Zn-based high-temperature brazing alloys, Zn–Sn alloy has been one of the preferred solders due to its low cost, superior mechanical properties, electrical and thermal conductivity [11, 12]. Besides, the poor corrosion resistance of zinc can be a disadvantage when the alloys are exposed to a corrosive environment [13, 14].

High-temperature solders are frequently used in optical components, automobile circuit boards, step soldering, assembling circuit modules. Requirements for high-temperature solders are melting temperature in the range of 260 to 400°C, softness to preserve joint structure in relieving thermal stress, small volume expansion in reflow process, good machinability, mechanical properties, electrical and thermal conductivity [2].

In recent studies, Zn–5Sn–2Cu–1.5Bi high temperature solder with 400°C melting temperature has been developed for soldering problems of functional materials [2, 15, 16]. In this study, small amounts of Al, Ag and Sb was added to the alloy to improve the solder. Then, the effects of these additions on the microstructure, thermal conductivity, and microhardness of ZSCB and ZSCB–0.05X (X = Al, Ag, Sb) solders were investigated. Zn has a melting temperature of 419.5°C. It also makes a strong reaction with copper and steel. The melting temperatures of alloying ele-

Table 1. Some thermal properties of Zn–5Sn–2Cu–1.5Bi and Zn–5Sn–2Cu–1.5Bi–0.05X (X = Al, Ag, Sb) alloys

Composition, wt %	Solidus temperature, K	Liquids temperature, K	Peak temperature, K	Melting range, K
Zn–2Cu–1.5Bi–5Sn	680.43	689.22	683.94	8.79
Zn–2Cu–1.5Bi–5Sn–0.05Sb	672.44	693.04	685.52	20.06
Zn–2Cu–1.5Bi–5Sn–0.05Al	678.03	691.52	685.15	13.49
Zn–2Cu–1.5Bi–5Sn–0.05 Ag	678.00	698.22	689.82	20.22

ments and Zn-based alloys can be adjusted to a suitable melting temperature between 350–500°C [17]. Sn and Al are traditional additions to form Zn–Sn [18, 19] and Zn–Al [20, 21] solders, which are widely used in electrical packaging and soldering of Al alloys. Studies of Zn–Cu solders used to join copper and steel at 350–500°C are scarce in the literature [22]. However, by adding small amounts of Cu, Bi and Sn to Zn alloys, the new ZSCB high temperature solder has been developed [15]. Considering all this information, ZSCB alloy is a promising high-temperature solder, and its detailed study is thought to be beneficial for special applications and better material design. Therefore, the aim of this study was to evaluate the microstructure, variation of thermal conductivity with temperature, melting properties and microhardness of ZSCB and ZSCB–0.05X (X = Al, Ag, Sb) alloys.

EXPERIMENTAL PROCESS

Specimen Preparation

A graphite crucible with a length of 12.0 mm OD × 8.0 mm ID × 50 mm was made using graphite rod. A 1.2 mm diameter hole was drilled in the bottom of the crucible to accommodate the thermal double alumina tube. Zn–5Sn–2Cu–1.5Bi and Zn–5Sn–2Cu–1.5Bi–0.05X (X = Al, Ag, Sb) alloys were melted separately in a vacuum furnace using 99.99% pure metals. The casting furnace is used to unidirectionally solidify the molten alloy into the crucible. The details of the experimental system can be seen in References [23–24].

Metallographic Processes

The samples were cut into small pieces transversely with the Micracut 151 off cutting tool. It was then embedded using a transparent thermoplastic resin. Grinding and polishing processes were carried out in Mikrotest Multipol Advanced automatic polishing machine. Before each polishing step, the samples were washed with green soap solution and ultrasonically cleaned for 5 min. In the last step, the samples were ultrasonically cleaned to remove the colloidal silica from the polished surface. The samples were then cleaned with ethanol and dried. After polishing, Zn–5Sn–2Cu–1.5Bi and Zn–5Sn–2Cu–1.5Bi–0.05X (X = Al, Ag, Sb) were etched in were etched with 40 g chromic acid (CrO_3), 10 mL hydrochloric acid (HCl), 1.5 g sodium sulphate (Na_2SO_4) in 200 ml water for 10–15 s and the samples were cleaned with 20% chromic acid in distilled water. Scanning Electron Microscopy (SEM) photographs of microstructure of Zn–5Sn–2Cu–1.5Bi and Zn–5Sn–2Cu–1.5Bi–0.05X (X = Al, Ag, Sb) alloys are shown in Fig. 1. Energy Dispersive X-Ray Analysis (EDX) composition analysis was used to obtain the phases of Zn–5Sn–2Cu–1.5Bi and Zn–5Sn–2Cu–1.5Bi–0.05X (X = Al, Ag, Sb) alloys and the EDX composition analysis were given in Figs. 2–5.

The Enthalpy of Fusion and the Specific Heat Change of the Materials

In this study three different compositions of ZSCB alloy system's melting temperature, phase transition temperature and enthalpy values were measured by using *Perkin Elmer* (Q 8000) model DSC device. Approximately 3.5 mg of material was prepared for each alloy. For each alloy, measurements were taken starting from room temperature up to 10 K/s with a heating rate of 773 K under nitrogen gas. Heat flow-temperature graphs for each system are given in Fig. 6 and Table 1. By using these graphs, the initial, final, and maximum melting temperatures and transition temperatures were determined.

Thermal Conductivity Measurements

A longitudinal linear heat flow apparatus was used for thermal conductivity measurements. Details of the system are given in [25].

From one-dimensional heat conduction equation by Fourier's law for steady state condition, the thermal conductivity (K) is defined as:

$$K = \frac{Q\Delta X}{A\Delta T}, \quad (1)$$

here Q is the net input power, flows through to the specimen that is taken as the difference between the input power with specimen and the input power without specimen for every measurement temperature ($Q = Q_{WS} - Q_{WOS}$), A is the cross-sectional surface area of the specimen ($A = \pi r^2$), normal to heat flow direction, $\Delta T = T_2 - T_1$ is the temperature difference between two points into the sample that determined

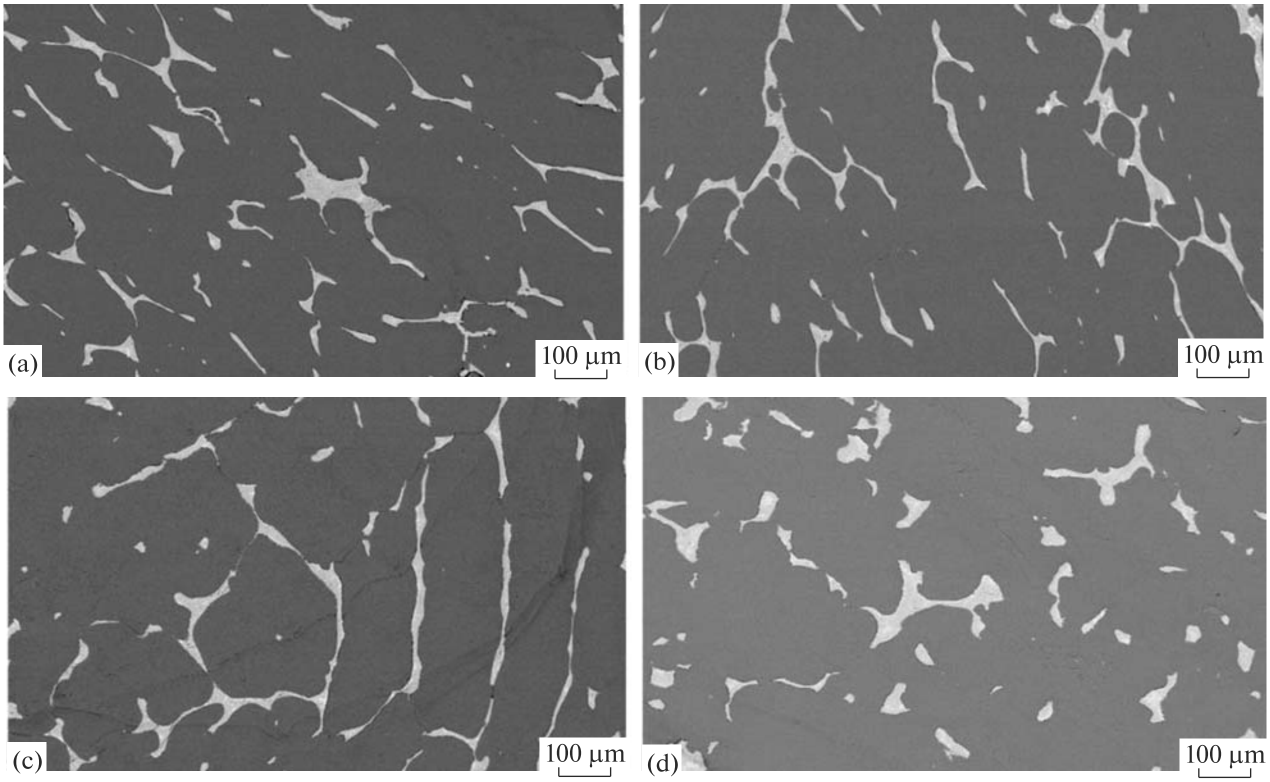

Fig. 1. SEM photographs of (a) Zn–2 wt % Cu–1.5 wt % Bi–5 wt Sn, (b) Zn–2 wt % Cu–1.5 wt % Bi–5 wt % Sn–0.05 wt % Al, (c) Zn–2 wt % Cu–1.5 wt % Bi–5 wt % Sn–0.05 wt % Ag, (d) Zn–2 wt % Cu–1.5 wt % Bi–5 wt % Sn–0.05 wt % Sb alloy systems.

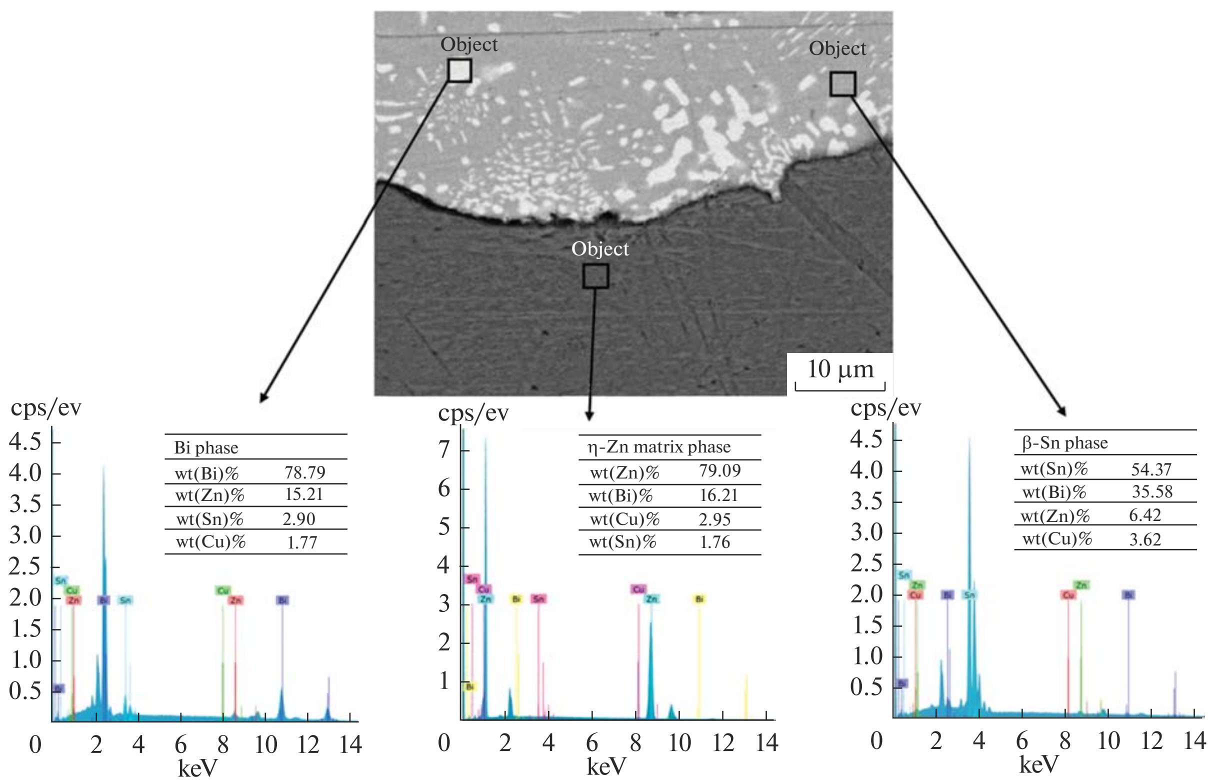

Fig. 2. SEM photographs and EDX composition analysis of Zn–2 wt % Cu–1.5 wt % Bi–5 wt % Sn.

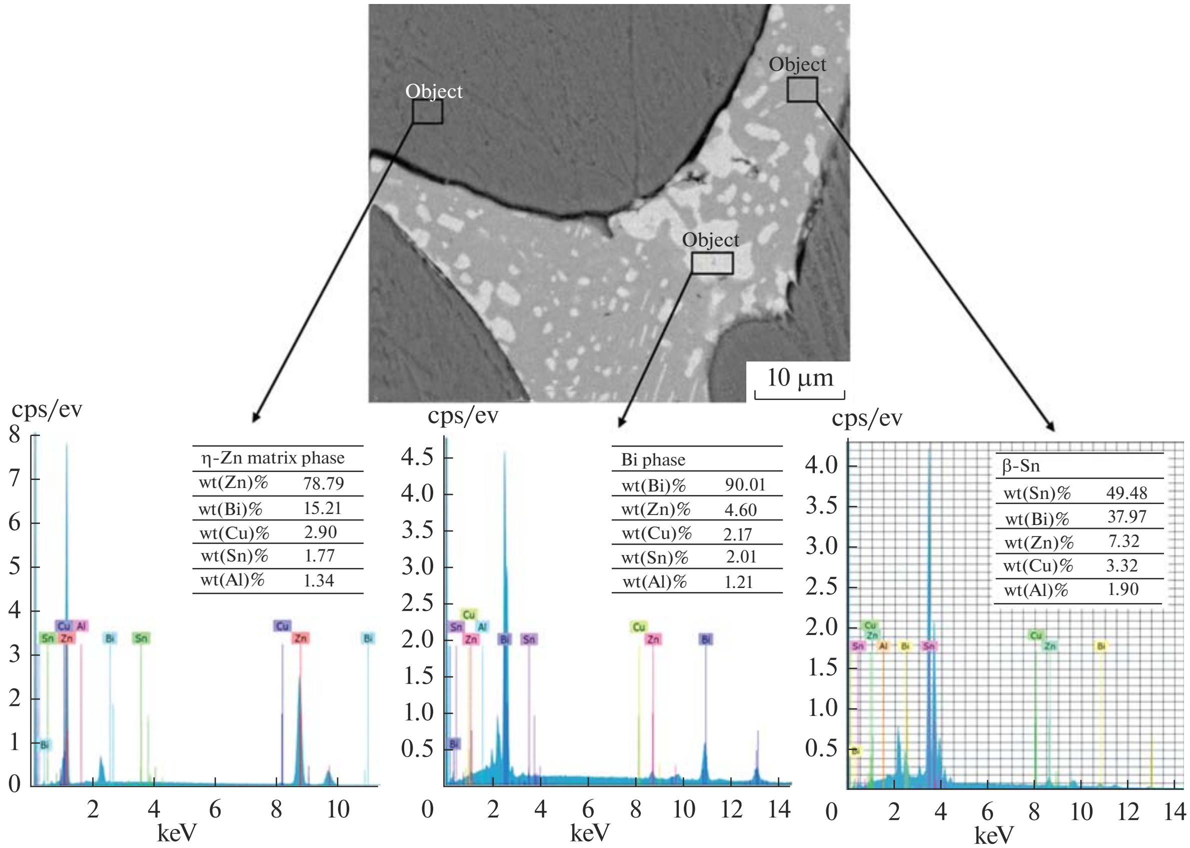

Fig. 3. SEM photographs and EDX composition analysis of Zn–2 wt % Cu–1.5 wt % Bi–5 wt % Sn–0.05 wt % Al.

with a data logger, and $\Delta X = X_2 - X_1$ is the distance between two measurement points that are obtained from the photos of the thermocouple's positions.

The sample was heated from room temperature to 20 K below the melting points of the alloys in 10 K steps and annealed for at least two hours for each step under steady-state conditions. During the experiment, a constant linear temperature gradient was obtained using hot and cold stages, and *K*-type thermocouples (0.5 mm diameter) were used to measure the temperatures of the sample. At each temperature value, constant current and potential difference measurements were made to determine the heat flow through the sample.

Measurements of Microhardness

Vickers method was used for microhardness measurements. A pyramid diamond tip that has a square sole and 136° edge angle was used in Future-Tech FM-700 type device. This diamond tip was pricked the surface of the sample with a load of 25 g and removed after 10 s. The trace's diagonals that occurred after the tip process, were measured and by using Eq. (1) Vickers microhardness values were calculated [26].

$$HV = 1.854x\frac{F}{d^2}. \quad (2)$$

Here *F* (kgf) is the applied force and *d* (mm) is the average bottom diagonal length.

This uncertainty is defined as *U*. *U* = ±2% for Zn–5Sn–2Cu–1.5Bi and Zn–5Sn–2Cu–1.5Bi–0.05X (X = Al, Ag, Sb) alloy system in 95% safety level (coverage factor *K* = 2). Table 2 shows the results for every alloy system.

RESULTS AND DISCUSSION

Microstructures

Figure 1 shows the representative SEM micrograph of Zn–5Sn–2Cu–1.5Bi and Zn–5Sn–2Cu–1.5Bi–0.05X (X = Al, Ag, Sb) high-temperature solders. Regarding the analysis of the EDX curves shown in Figs. 2–5, the microstructure of ZSCB and ZSCB–0.05X (X = Al, Ag, Sb) solder consists of light gray η-Zn matrix, fiber-like β-Sn and white spherical Bi phases. As shown in Fig. 1 adding 0.05 wt % Al and Ag does not change the microstructure of present phases but adding 0.05 wt % Sb really increases the sphericity ratio of Bi because Bi and Sb are completely soluble into each other.

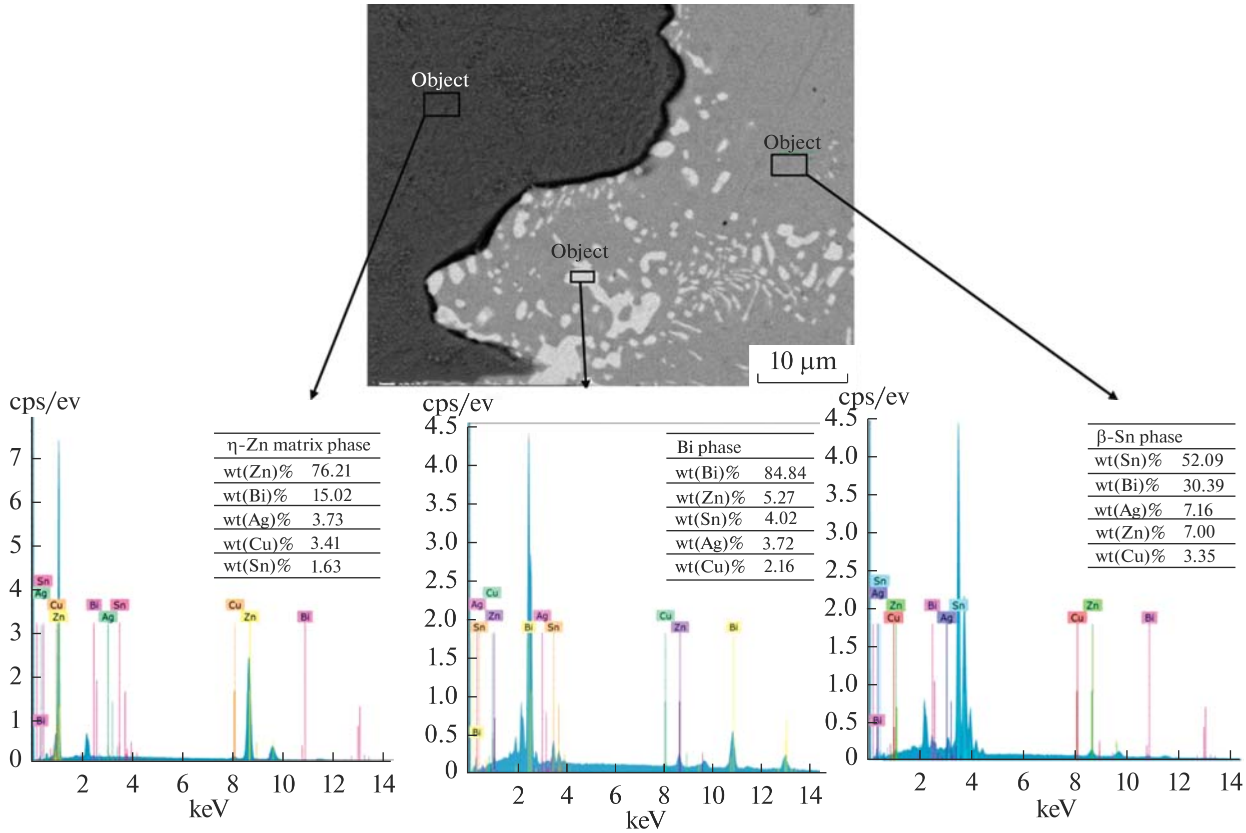

Fig. 4. SEM photographs and EDX composition analysis of Zn–2 wt % Cu–1.5 wt % Bi–5 wt % Sn–0.05 wt % Ag.

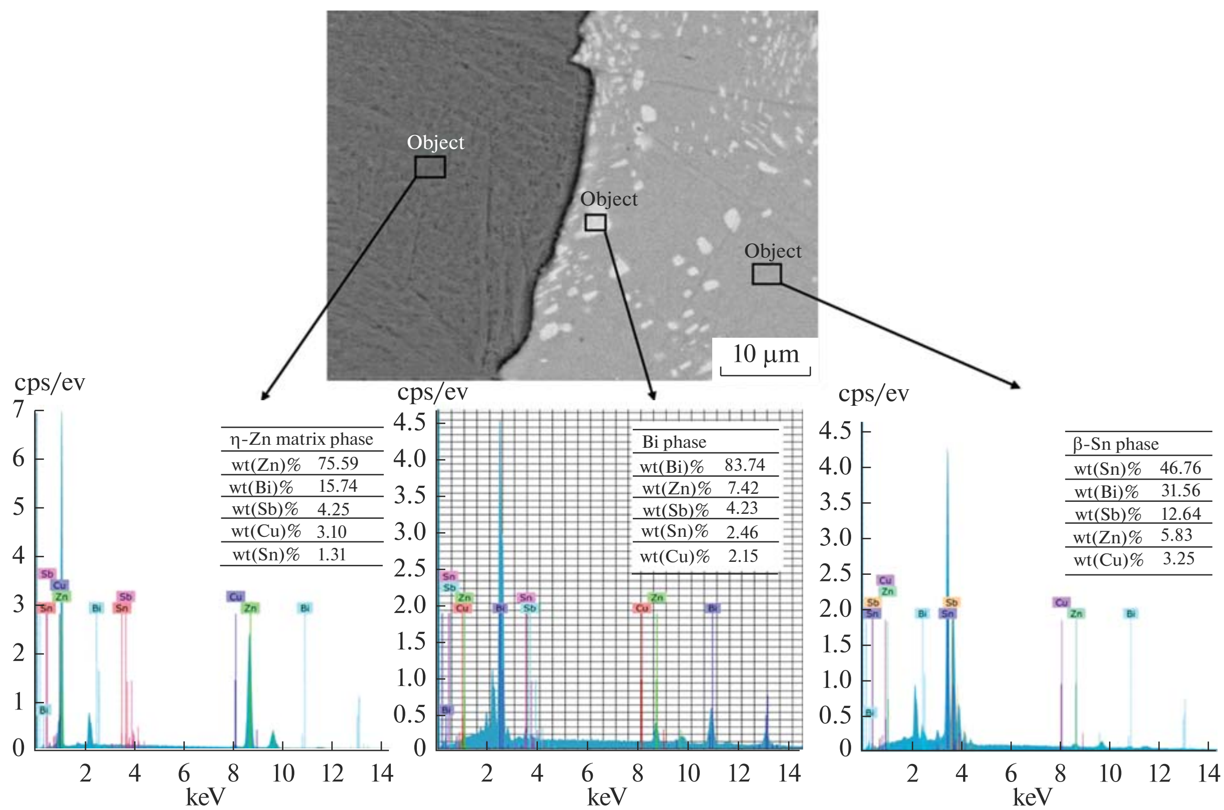

Fig. 5. SEM photographs and EDX composition analysis of Zn–2 wt % Cu–1.5 wt % Bi–5 wt % Sn–0.05 wt % Sb.

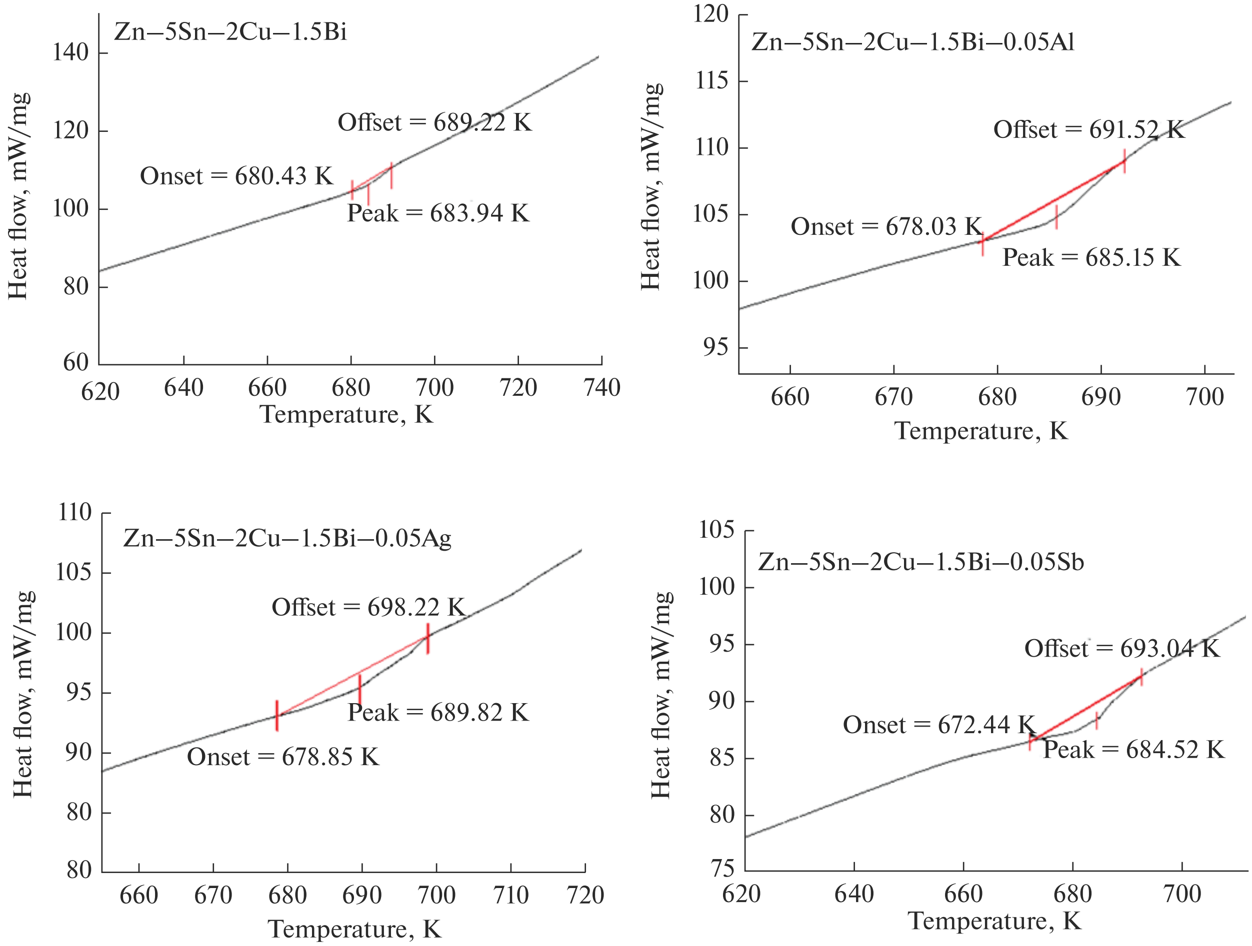

Fig. 6. DSC thermogram of Zn–5Sn–2Cu–1.5Bi and Zn–5Sn–2Cu–1.5Bi–0.05X (X = Al, Ag, Sb) alloy systems at heating rates of 10°C/min.

The Enthalpy of Fusion and the Specific Heat Change of Material

DSC analysis was carried out in order to investigate the fundamental thermal reactions of ZSCB high-temperature solder during heating. The solidus temperature (T_S), liquidus temperature (T_L), and melting range ($\Delta T = T_L - T_S$) of these alloys are calculated and presented in Table 1.

Additions of Al, Ag and Sb have obvious effects on the melting property of ZSCB solder during the heating process. When 0.05% by weight Al, Ag and Sb metals were added to the ZSCB high-temperature solder

Table 2. The microhardness values of solid phases for the Zn–5Sn–2Cu–1.5Bi and Zn–5Sn–2Cu–1.5Bi–0.05X (X = Al, Ag, Sb)

Composition, wt %	Microhardness HV, kg mm^{-2}	
Zn–2Cu–1.5Bi–5Sn	η-Zn matrix phase	61.94 ± 5.91
	β-Sn phase	30.61 ± 5.07
Zn–2Cu–1.5Bi–5Sn–0.05Al	η-Zn matrix phase	73.62 ± 5.25
	β-Sn phase	31.04 ± 2.52
Zn–2Cu–1.5Bi–5Sn–0.05Ag	η-Zn matrix phase	74.98 ± 6.52
	β-Sn phase	34.35 ± 5.42
Zn–2Cu–1.5Bi–5Sn–0.05Sb	η-Zn matrix phase	84.23 ± 5.15
	β-Sn phase	38.77 ± 3.81

Table 3. Thermal conductivity values of high-temperature lead-free alloys

Materials	Melting temperature, K	Thermal conductivity at the melting temperature, K, W/mK	Thermal temperature coefficient, α_{TTC}, $K^{-1} \times 10^{-3}$
Zn–5Sn–2Cu–1.5Bi	683.94	20.74	2.057
Zn–5Sn–2Cu–1.5Bi–0.05Al	685.15	33.56	1.744
Zn–5Sn–2Cu–15Bi–005Ag	689.82	33.56	1.809
Zn–5Sn–2Cu–1.5Bi–0.05Sb	684.89	27.66	1.861
Au–20Sn [1]	–	57	–
Au–12Ge [1]	–	44	–
Au–3Si [1]	–	27	–
Sn–5Sb [1]	–	48	–
Pb–5Sn [1]	–	23	–
Zn–(10–30)Sn [1]	–	100~110	–
Bi–11Ag [1]	–	~9	–
Pure Zn [28]	692.70	49.50	–
Pure Sn [28]	505	30	–
Pure Cu [28]	1.356	165.60	–
Pure Bi [28]	545	17.10	–
Pure Al [28]	933	94.03	–
Pure Ag [28]	1.234	174.80	–
Pure Sb [28]	904	21.8	–

alloy, it decreased the liquidus temperature value of the alloys and increased the solidus temperature value. As a result, the melting temperature range of ZSCB–0.05X (X = Al, Ag, Sb) alloys has expanded. Table 1 also illustrates that the melting temperature range of ZSCB–0.05Al solder lies in the range of 13°C, which is lower than 20°C for ZSCB–0.05Ag and ZSCB–0.05Sb high-temperature solder. ZSCB–0.05X (X = Al, Ag, Sb) solders have a small melting temperature range, which could help them avoid manufacturing issues like vibration sensitivity during wave soldering. Furthermore, because of alloy shrinkage, it can reduce the likelihood of fillet lifting phenomena, the inclination toward porosity, and hot tearing. Consequently, among the Zn–5Sn–2Cu–1.5Bi–0.05X (X = Al, Ag, Sb) alloys, ZSCB–0.05Al has the lowest melting temperature range [2].

Thermal Conductivity Variation with Temperature

The conductivity of Zn–Sn alloys was compared with the other high temperature solders, which is shown in Table 3. The *K* values for the Zn–Sn alloys exceeds 100 W/mK, while the *K* values for Pb–5Sn and Au–20Sn alloys are 36 and 59 W/mK, respectively. Bismuth-based alloys are known to have the worst thermal conductivity which are smaller than 10 W/mK. Thus, the Zn–Sn alloys have a great advantage as die-attachment solder that must possess excellent mechanical and thermal properties. In this study, the variation of thermal conductivity with temperature for ZSCB alloy adding Al, Ag and Sb metals was investigated to create different alternatives to die-attachment solders.

In Fig. 7, thermal conductivity-temperature graphs for the ZSCB and ZSCB–0.05X (X = Al, Ag and Sb) alloys solid phases have been plotted, and the data are given in Table 4. As can be seen from Fig. 7, the variations of *K* wit *T* for ZSCB and ZSCB–0.05X (X = Al, Ag and Sb) alloys linear decreased.

The thermal temperature coefficients (α_{TTC}) for the ZSCB and ZSCB–0.05X (X = Al, Ag, Sb) were also calculated as 2.05, 1.74, 1.80 and 1.86 ($\times 10^{-3}$) K^{-1}, respectively from Fig. 7 and are also given in Table 3.

When Table 3 is examined, adding of 0.05 wt % Ag and Al and increased about 62 and 32% their *K* values, respectively according to the *K* value of ZSCB high-temperature solder alloy. The *K* values of pure Ag, Al and Sb at their melting temperature are 174.80 [27], 94.03 [27] and 21.8 [27] W/mK, respectively. Ag and Al are good conductor, and the Sb is poor conductor. Even with the addition of trace amounts of Ag and Al to the ZSCB alloy greatly increased the *K* value of the ZSCB alloy. For this reason, the ZSCB–0.05Ag and ZSCB–0.05Al alloys can be preferred as an alternative to die-attachment solders alloys, which should have excellent thermal properties.

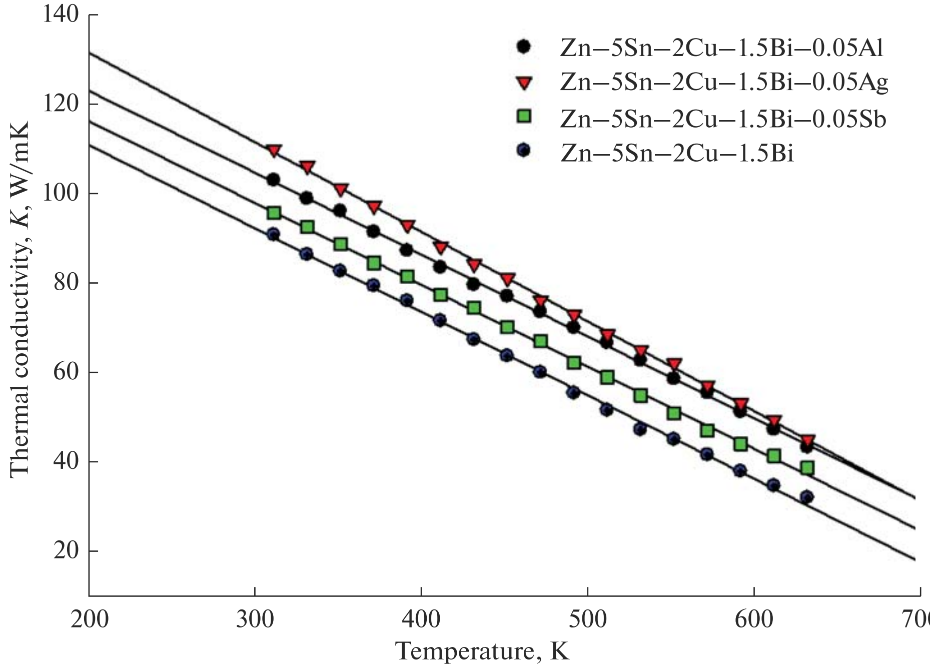

Fig. 7. The thermal conductivity variations with temperature alloys Zn–5Sn–2Cu–1.5Bi and Zn–5Sn–2Cu–1.5Bi–0.05X (X = Al, Ag, Sb).

Table 4. The experimental data in the measurement of thermal conductivity variations with temperature for the Zn–5Sn–2Cu–1.5Bi and Zn–5Sn–2Cu–1.5Bi–0.05X (X = Al, Ag, Sb) alloys

Temperature *T*, K	Thermal conductivity *K*, W/mK			
	ZSCB	ZSCB–0.05Ag	ZSCB–0.05Al	ZSCB–0.05Sb
313	90.62	109.78	102.77	95.58
333	86.18	105.99	98.67	92.33
353	82.49	101.01	95.91	88.54
373	79.23	97.12	91.26	84.34
393	75.87	92.87	87.06	81.27
413	71.40	88.03	83.34	77.23
433	67.21	84.10	79.42	74.33
453	63.54	80.95	76.85	69.99
473	59.89	76.03	73.38	66.88
493	55.29	72.79	69.85	62.04
513	51.46	68.42	66.52	58.86
533	47.11	64.89	62.56	54.76
553	44.93	61.96	58.46	50.73
573	41.48	57.06	55.31	46.87
593	37.81	53.02	51.12	43.97
613	34.56	49.39	47.15	41.28
633	31.94	44.93	43.18	38.65

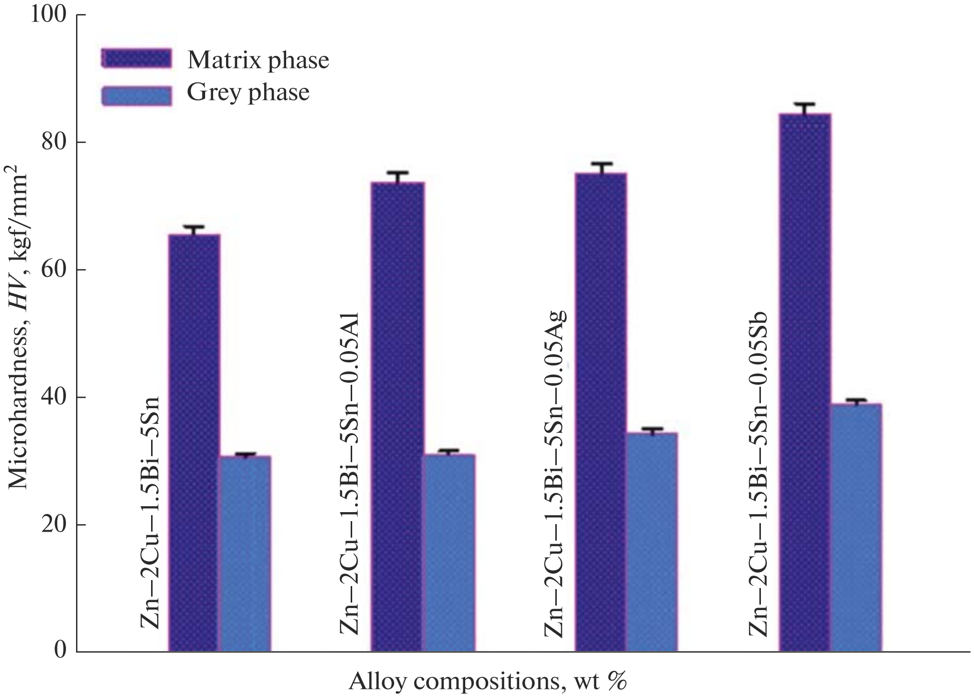

Fig. 8. Microhardness value (*H*) for Zn–2Cu–1.5Bi–5Sn and Zn–2Cu–1.5Bi–5Sn–0.05X (X = Al, Ag, Sb) alloys.

Variations of HV with Composition of Phases

Microhardness of the alloys depends upon various conditions like microstructure, shape of the phases, presence of hard compound phases in solder matrix, solubility limit as well as grain size, etc. In the present study, the *HV* test was performed to observe the *HV* dependence on the microstructural changes.

As mentioned above, adding 0.05 wt % Al, Ag and Sb to the ZSCB alloy, which is a high temperature solder alloy affected the microstructure of the ZSCB alloy. When the microstructure photographs in Figs. 2–5 are examined, it is seen that main three phases are exist of ZSCB and ZSCB–0.05X (X = Al, Ag, Sb) alloys. Microhardness value was not determined from these phases because the grain sizes of the Bi-rich phase were very small. The microhardness values of the η-Zn matrix and β-Sn phases for each alloy are given in Table 2. Also Fig. 8 shows the microhardness results with standard deviation as a function of alloy composition.

According to the EDX analysis, it was determined that dark grey phase is η-Zn matrix phase and light grey is β-Sn phase. In η-Zn matrix phase (the dark grey phase) where the zinc is the majority, microhardness values were taken from 10 different regions for 10 s with 25 gr load. As seen in Table 2, while the microhardness value of the η-Zn matrix phase in the ZSCB alloy was 61.94 kg mm^{-2}, a significant increase was observed in the microhardness values of the alloys obtained when Al, Ag and Sb were added at a weight ratio of 0.05 to this alloy. When 0.05 wt % Al and Ag were added to the ZSCB alloy, the microhardness value of the η-Zn matrix phase increased by about 19 and 21% respectively, while this value increased by 36% when 0.05 wt % Sb was added.

In this study, the microhardness value of the ZSCB alloy was found to be 61.94 ± 5.91 kg mm^{-2}, while in the study by Fei Xing et al. [2], this value was found to be 58(±3) kg mm^{-2}. This shows that the obtained results agree with the literature. In the study by Fei Xing et al. [2], while the elements added to the ZSCB alloy increased the microhardness value by 13–17%, the additives made in this study increased the microhardness value by 19–36%. The microhardness values of Al, Ag and Sb metals doped to the ZSCB alloy are 30.04 kg mm^{-2} [28], 67.57 kg mm^{-2} [29] and 77.28 kg mm^{-2} [30] respectively. As seen in Table 2, the microhardness value of the doped elements is higher than the microhardness value of the ZSCB alloy, which increased the microhardness values of the ZSCB–0.05X (X = Al, Ag, Sb) alloys. When 0.05 Al in weight was doped to the ZSCB alloy, the microhardness value of the η-Zn matrix phase was 73.62 ± 5.25 kg mm^{-2}, while the microhardness value of the β-Sn phase was 31.04 ± 2.52 kg mm^{-2}. When the Zn–Al [31] binary phase diagram is examined, it is seen that 0.7% Al in weight is dissolved in Zn at the eutectic temperature (550 K). Al metal dissolved in the ZSCB alloy increased the microhardness value of the η-Zn matrix phase of the alloy by 19%, while it did not have a significant effect on the microhardness value of the β-Sn phase. In the ZSCB–0.05Ag system, the microhardness value of the η-Zn matrix phase is 74.98 ± 6.52 kg mm^{-2}, while the microhardness value of the β-Sn phase is 34.35 ± 5.42 kg mm^{-2}. When Zn–Ag [31] binary phase diagram is examined, it is seen that 3% Ag is dissolved in Zn at eutectic temperature (704 K). Ag dissolved in the ZSCB alloy increased the microhardness value of the η-Zn matrix phase of the alloy by 21%, while it increased the microhardness value of the β-Sn phase by 12%. In the ZSCB-0.05Sb system, the microhardness values of the η-Zn matrix and β-Sn phases were determined as 84.23 ± 5.15 and 38.77 ± 3.81 kg mm^{-2}, respectively. When Zn–Sb [31] phase diagram is examined, it is seen that there is no Sb solubility in Zn. However, Bi–Sb [31] phase diagram is an isomorphic phase diagram with full solubility. Antimony is among hard metals with a microhardness value of 77.28 kg mm^{-2} [30]. Antimony dissolved in the ZSCB alloy, increased the microhardness value of the η-Zn matrix phase by 36% and the microhardness value of the β-Sn phase by 26% in the ZSCB–0.05Sb alloy.

CONCLUSIONS

Following conclusions can be made based on the results:

(1) As determined by EDX, the microstructure of ZSCB and ZSCB–0.05X (X = Al, Ag, Sb) solder alloys consist of a light gray—Zn matrix, fiber-like—Sn, and white spherical Bi phases.

(2) The addition of 0.05 percent by weight Al, Ag, and Sb metals to the ZSCB high-temperature solder alloy reduced the liquidus temperature value while increasing the solidus temperature value. As a result, the melting range of ZSCB–0.05X (X = Al, Ag, Sb) solder alloys have increased.

(3) Adding 0.05 percent by weight of Ag and Al and Sb metals are added into the ZSCB high-temperature solder alloy increased the *K* values of the alloys by 62 and 32 percent, respectively.

(4) Existence of 0.05 wt percent Al, Ag and Sb into the ZSCB alloy increased the *HV* value of the η-Zn matrix phase by 19, 21 and 36 percent, respectively.

FUNDING

Nevşehir Hacı Bektaş Veli University Research Foundation was provided the funding of this study under Contract No: TDP18F38. The researchers thank to the university for the support.

CONFLICT OF INTEREST

The authors of this work declare that they have no conflicts of interest.

REFERENCES

1. Suganuma, K., Kim, S.J., and Kim, K.S., *J. Miner., Met. Mater. Soc.,* 2009, vol. 6, p. 64.
2. Xing, F. and Qiu, X.M., *J. Mater. Eng. Perform.,* 2015, vol. 24, p. 1679.
3. Rödel, J., Jo, W., Seifert, K.T.P., Anton, E.M., and Granzow, T.J., *J. Am. Ceram. Soc.,* 2009, vol. 92, p. 1153.
4. Prasatkhetragarn, A., Unruan, M., Ngamjarurojana, A., Laosiritaworn Y., Ananta, S., Yimnirun, R., and Cann, D.P., *Curr. Appl. Phys.,* 2009, vol. 9, no. 5, p. 1165.
5. Kim, J.I. and Miyazaki, S., *Acta Mater.,* 2005, vol. 53, p. 4545.
6. Du, H.L., Zhou, W.C., Luo, F., Zhu, D.M., Qu, S.B., and Pei, Z.B., *J. Appl. Phys.,* 2009, vol. 105, p. 124104.
7. Cheng, H.L., Zhou, W.C., Du, H.L., Luo, F., and Zhu, D.M., *Trans. Nonferrous Met. Soc. China,* 2013, vol. 23, p. 2984.
8. Li, M.G., Sun, D.Q., Qiu, X.M., Sun, D.X., and Yin, S.Q., *Mater. Sci. Eng., A,* 2006, vol. 424, nos. 1–2, p. 17.
9. Gancarz, T., Pstrus, J., Fima, P., and Mosinska, S., *J. Mater. Eng. Perform.,* 2012, vol. 21, p. 599.
10. Kroupa, A., Andersson, D., Hoo, N., Pearce, J., Watson, A., and Dinsdale, A.T., *J. Mater. Eng. Perform.,* 2012, vol. 21, no. 5, p. 629.
11. Takahashi, T., Komatsu, S., Nishikawa, H., and Takemoto, T., *J. Electron. Mater.,* 2010, vol. 39, p.1241.
12. Song, J.M., Lin, M.J., Hsieh, K.H., Pai, T.Y., Lai, Y.S., and Chiu, Y.T., *J. Electron. Mater.,* 2013, vol. 42, no. 9, p. 2813.
13. Song, J.M., Tsai, C.H., and Fu, Y.P., *Corros. Sci.,* 2010, vol. 52, p. 2519.
14. Park, S.W., Sugahara, T., Kim, K.S., and Suganuma, K., *J. Alloys Compd.,* 2012, vol. 542, p. 236.
15. Qiu, X.M., Xing, F., Ma, F., and Bai, Y., CN Patent 201110341677.8, 2013.
16. Xing, F., Qiu, X.M., Wu, A.M., and Wen, Y.H., *Proc. International Conference on Brazing, Soldering and Special Joining Technologies,* Beijing, June 9–13, 2014, p. 168.
17. Xing, F., Qiu, X.M., and Li, Y.D., *Trans. Nonferrous Met. Soc. China,* 2015, vol. 25, p. 879.
18. Kim, S., Kim, K.S., Kim, S.S., and Suganuma, K., *J. Electron. Mater.,* 2009, vol. 38, no. 2, p. 266.
19. Mahmudi, R. and Eslami, M., *J. Mater. Sci.: Mater. Electron.,* 2011, vol. 22, no. 8, p. 1168.
20. Dai, W., Xue, S., Lou, J., Lou, Y., and Wang, S., *Trans. Nonferrous Met. Soc. China,* 2012, vol. 22, no. 1, p. 30.
21. Xiao, Y., Ji, H., Li, M., Kim, J., and Kim, H., *Mater. Des.,* 2013, vol. 47, p. 717.
22. Qiu, X., Yi, Y., and Liu, C., *Welding and Joining,* 1993, vol. 6, p. 5.
23. Gündüz, M. and Hunt, J.D., *Acta Metall.,* 1985, vol. 33, p. 1651.
24. Maraşlı, N. and Hunt, J.D., *Acta Metall.,* 1996, vol. 44, p. 1085.
25. Demir, M., Aksöz, S., Öztürk, E., and Maraşlı, N., *Metall. Mater. Trans. B,* 2014, vol. 45, p. 1739.

26. Callister, W.D. and Rethwisch, D.G., *Fundamentals of Materials Science and Engineering: An Integrated Approach,* John Wiley and Sons, 2008, p. 175.

27. Brandes, E.A. and Brook, G.B., *Smithells Metals Reference Book,* Elsevier, 1998, vol. 14.

28. Sivasankaran, S., Ramkumar, K.R., Ammar, H.R., Al-Mufadi, F.A., Alaboodi, A.S., and Irfan, O.M., *J. Mater. Process. Technol.,* 2021, vol. 292, p. 117063.

29. El-Bahay, M.M., El Mossalamy, M.E., Mahdy, M., and Bahgat, A.A., *J. Mater. Sci.: Mater. Electron.,* 2004, vol. 15, p. 519.

30. El-Bahay, M.M., El Mossalamy, M.E., Mahdy, M., and Bahgat, A.A., *Phys. Status Solidi A,* 2003, vol. 198, no. 1, p. 76.

31. Hansen, M., *Constitution of Binary Alloys,* New York: McGraw-Hill, 1958.